The evolution of carbon oxidation state during secondary organic aerosol formation from individual and mixed organic precursors

Yunqi Shao[1], Aristeidis Voliotis[1,2], Mao Du[1,6], Yu Wang[1,5], Thomas J. Bannan[1], Jacqueline Hamilton[3], M. Rami Alfarra[1,2] [4], Gordon McFiggans[1]

[1]School of Earth and Environmental Science, University of Manchester, Manchester, M13, 9PL, UK
[2]National Centre for Atmospheric Science (NCAS), University of Manchester, Manchester, M13 9PL, UK
[3] Wolfson Atmospheric Chemistry Laboratories, Department of Chemistry, University of York, York, YO105DD, UK
[4] Now at Qatar Environment and Energy Research Institute, Hamad Bin Khalifa University, Doha, Qatar
[5] now at School of Geosciences, University of Edinburgh, Edinburgh, EH9 3FF, UK
[6] now at School of Geography Earth and Environment Sciences, University of Birmingham, Birmingham B15 2TT, UK

Correspondence to: Yunqi.Shao (Yunqi.Shao@Manchester.ac.uk)

Abstract

This study reports the average carbon oxidation state ($\overline{OSc}$) of secondary organic aerosol (SOA) particles formed from the photo-oxidation of *o*-cresol, α-pinene, isoprene and their mixtures, representative anthropogenic and biogenic precursors, in the Manchester Aerosol Chamber. Three independent mass spectrometric techniques, including two online instruments, high resolution time-of-flight Aerodyne Aerosol Mass Spectrometers (HR-ToF-AMS) and Filter Inlet for Gases and AEROsols coupled to an Iodide high-resolution time of flight chemical ionisation mass spectrometer (FIGAERO-CIMS), and one offline technique, ultra-high-performance liquid chromatography-high resolution mass spectrometry (UHPLC-HRMS) , were employed to characterise chemical composition of SOA and derive average $\overline{OSc}$ in mixtures of α-pinene/isoprene, *o*-cresol/isoprene, α-pinene/ *o*-cresol and α-pinene/*o*-cresol/isoprene system. This paper firstly reports the detailed analysis of particle average $\overline{OSc}$ during SOA formation in mixed anthropogenic and biogenic systems using two online and one offline mass spectrometry techniques simultaneously.

Across single precursor experiments, $\overline{OSc}$ generally declined with increasing SOA mass, suggesting with a shift from highly oxygenated, low-volatility products at early stages toward more semi-volatile, less oxidised compounds at higher particle mass loading. This behaviour was robust across different initial precursor concentrations, implying that SOA growth is dominated by partitioning dynamics rather than initial precursors ' reactivity.

Moreover, comparisons across analytical techniques demonstrate systematic differences, with FIGAERO-CIMS consistently reported higher $\overline{OSc}$, UHPLC-HRMS (negative mode) aligned more closely with FIGAERO-CIMS, while HR-ToF-AMS underestimated $\overline{OSc}$ due to its inability to resolve nitrogen containing species.

Furthermore, correcting for the oxidation state of nitrogen ($\overline{OS_N}$) significantly reduced $\overline{OSc}$ estimates in *o*-Cresol experiments, likely reflecting the strong influence of CHON compound.

Mixture precursor experiments reveals the isoprene suppressed the formation of highly oxygenated α-pinene products through OH scavenging and RO_2 competition, lowering $\overline{OSc}$ in mixed systems. In contrast, α-pinene/*o*-Cresol mixtures showed elevated $\overline{OSc}$, likely contributed by the cross interaction between precursor's driven RO_2 forming multifunctional accretion products. The ternary mixture evolved to intermediate $\overline{OSc}$ values between the single precursor experiment, which could imply a balance between OH scavenging, RO_2 competition, and cross interaction reaction.

1. Introduction

The formation and evolution of secondary organic aerosol (SOA) from mixtures of volatile organic compounds (VOCs) play an important role to understanding ambient organic aerosol (OA) composition. While early chamber studies predominantly investigated SOA formation from individual precursors (Lee et al., 2011; Winterhalter et al., 2003; Pandis et al., 1991; Hoffmann et al., 1997; Eddingsaas et al., 2012; Kroll et al., 2005a; Ahlberg et al., 2017; Pullinen et al., 2020; Kroll et al., 2005b), more recent research has shifted toward exploring multi-precursor systems(Han et al., 2025; Chen et al., 2025; Cui et al., 2024), reflecting the chemical complexity of the real atmosphere, where anthropogenic and biogenic VOCs coexist and interact. These interactions can significantly alter SOA yields, volatility distributions, and chemical composition, often through competition for oxidants or formation of cross-products.

Mcfiggans et al. (2019) demonstrated that isoprene reduced SOA mass and yield by scavenging OH radicals and their derived products, thereby suppressing the formation of highly oxygenated molecules (HOMs) from α-pinene oxidation and increasing the overall volatility of the mixture. However, more recent findings by Voliotis et al. (2022a) showed that although the addition of isoprene altered the chemical composition of the SOA and suppressed certain α-pinene-derived products, the overall volatility distribution remained largely unchanged likely due to the formation of new products with comparable volatility distributions. Li et al. (2022) further demonstrated that isoprene can suppress SOA yields from anthropogenic aromatics (e.g., toluene, p-xylene) through OH scavenging, emphasizing the importance of VOC competition. Additionally, Zhao et al. (2025) highlighted mechanistic interactions in mixed biogenic systems, showing that in α-pinene and limonene mixtures, limonene-derived RO_2 radicals and oxidation products facilitated the formation of cross-dimers, enhancing SOA yields. These findings highlighted the importance of the mechanistic interaction between the oxidation products of the precursor in understanding SOA formation in the presence of multiple VOCs.

Despite significant advances, the chemical characterization of SOA from mixed VOC systems remains challenging. OA in the ambient atmosphere comprises thousands of compounds, including hydrocarbons, alcohol, aldehydes and carboxylic acids, with a small fraction (~10-30%) of these capable of being characterised at a molecular level by current techniques

70   (Hoffmann et al., 2011). Moreover, the chemical complexity of OA increases if there are

71   multiple OA sources (both anthropogenic and biogenic sources) that contribute to OA

72   formation. A current lack of detailed chemical characterisation of these organic species makes

73   it difficult to track the OA sources, understand their atmospheric processes and mitigate their

74   adverse impacts. The majority of ambient SOA is generated by oxidation of VOCs with the

75   dominant prevailing oxidants, hydroxyl radicals (OH), ozone (O_3) and nitrate radicals (NO_3)

76   with their relative contributions varying throughout the day and night, leading to low-volatility

77   products that partition into the particle phase (Atkinson, 2004). As SOA ages, its composition

78   evolves through multi-generational oxidation (Kroll et al., 2005a; Ahlberg et al., 2017;

79   Pullinen et al., 2020)

80

81   A useful framework to describe this chemical evolution is the average carbon oxidation state

82   ($\overline{OSc}$), which increases with the extent of oxidation (Kroll et al. (2011). According to the

83   valence rule, a simplified expression for the average $\overline{OSc}$ of organic mixtures in terms of the

84   molar oxygen to carbon (O/C) and hydrogen to carbon (H/C) ratios is shown in Equation 1.

85

86    $$\overline{OSc} = 2 * \frac{O}{C} - \frac{H}{C} \qquad (1)$$

87

88   Changes in carbon oxidation state provide a valuable insight into the oxidation dynamics

89   associated with the formation and evolution of ensemble SOA. For example, the $\overline{OSc}$ generally

90   increases by functionalisation, which can frequently occur in VOC oxidation leading to C-O

91   bonds, for example, replacing C-H or unsaturated C-C bonds. An exception to this is when

92   functionalisation leads to the addition of nitro groups forming a C-N bond, and $\overline{OSc}$ remains

93   the same. In contrast, the average $\overline{OSc}$ remains unchanged by oligomerisation, which may

94   occur after functionalisation and fragmentation reaction (Kroll et al., 2015). On the other hand,

95   change in the average $\overline{OSc}$ of particulate organic molecules is also associated with their

96   volatility, which can strongly influence gas-particle partitioning, resulting in changes in the

97   ensemble chemical composition and increase of OA mass concentration. In general, the overall

98   volatility will decrease with more functionalised molecules and increase with fragmentation

99   (Daumit et al., 2013). Changes in $\overline{OSc}$ and atomic ratios (H/C and O/C ratios) upon SOA mass

loading can therefore be useful tools in identifying the key process in the atmospheric ageing of SOA.

In our chamber studies of SOA formation in mixtures of α-pinene, isoprene and *o*-cresol, we have reported the chemical composition of SOA by offline ultra-high-performance liquid chromatography orbitrap mass spectrometry (Voliotis et al., 2022b; Shao et al., 2022a). Oxidation products from the high yield precursor, α-pinene, dominated SOA in its mixtures, whilst isoprene derived compounds made a negligible contribution. Interactions in the oxidation of mixed precursors were found to lead to products uniquely found in the mixtures. In this study, we expand the investigation to report online measurements from the high resolution time-of-flight Aerodyne Aerosol Mass Spectrometers (HR-ToF-AMS) and Filter Inlet for Gases and AEROsols coupled to an Iodide high-resolution time of flight chemical ionisation mass spectrometer (FIGAERO-CIMS; Lee et al. (2014)) to measure the near real-time atomic ratios and derive the oxidation state of SOA during these experiments. The HR-ToF-AMS technique had been widely used for analysing the non-refractory aerosol chemical composition (Aiken et al., 2008; Shilling et al., 2009; Presto et al., 2009; Chhabra et al., 2010; Docherty et al., 2018) and can provide sensitive and online measurements of SOA elemental composition. The FIGAERO-CIMS was used to provide measurements of both gas-phase and particle-phase chemical constituents of organic aerosols in real time. Both instruments have limitations precluding molecular identification (electron impact ionisation in the HR-ToF-AMS leads to extensive fragmentation and the CIMS cannot resolve structural isomers or isobaric compounds (Lee et al., 2014)). Nevertheless, both online instruments can provide the time profile of atomic ratios of the SOA and derived average carbon oxidation state to add interpretation of the evolution of organic compounds to the offline measurement by ultra-high-performance liquid chromatography-high resolution mass spectrometry (UHPLC-HRMS.

The present study investigates the evolution of the average $\overline{OSc}$ during SOA formation from single precursors and their mixture system, with a focus on linking the $\overline{OSc}$ dynamics to underlying chemical mechanism. Specifically, five key questions were addressed and examined in this study:

i. How does $\overline{OSc}$ vary with SOA mass loading to provide insights into volatility and aging process?

131   ii.   How do different initial precursor reactivities influence $\overline{OSc}$ evolution in single
132   precursor experiments?
133   iii.   How consistent are $\overline{OSc}$ estimates across different analytical techniques, and what
134   does the respective bias imply?
135   iv.   How do the nitrogen-containing compounds affect the $\overline{OSc}$ estimation, particularly in
136   systems that contain abundant CHON products?
137   v.   How does the mixing of precursors impact on the oxidation trajectories compared to
138   the single precursor system, using $\overline{OSc}$ as a diagnostic metric?

139

140

141   To answer these questions, a series of photochemical oxidation experiments were designed and
142   conducted to produce SOA from the selected VOCs (α-pinene, isoprene and o-Cresol) and their
143   mixtures in the presence of neutral seed particles (ammonium sulphate) and NO_x. The
144   experimental program thereby included three single precursor experiments, three binary
145   precursor mixtures and one ternary mixture of precursors. For studying the effect of the initial
146   VOC concentration on the particle composition and carbon oxidation state of SOA evolution,
147   here we also conduct single precursor experiments at half and third initial concentration (and
148   hence reactivity towards the dominant oxidant in our experiments, the hydroxyl radical, OH).
149   However, experiments with o-cresol a third reactivity and isoprene a half reactivity are not
150   reported as a result of technical difficulties. The HR-ToF-AMS and FIGAERO-CIMS
151   continuously sampled and measured the SOA particles throughout the experiment and the
152   entire chamber contents were flushed through a filter for collection of the aerosol at the end of
153   the experiment for subsequent offline analysis by UHPLC-HRMS.

154

155

2. Materials and Methods

2.1. Experimental Procedure

The concept of iso-reactivity towards OH radicals was used to select the initial VOC
concentrations in each experiment to enable comparable initial turnover of VOCs in the mixture

162 with respect to OH radicals, such that the oxidation products from each VOCs would make
163 comparable contributions at the chosen concentration and experimental conditions at the
164 beginning of experiment. The injected mass of VOC precursors was calculated based solely on
165 their reactivity with OH radicals (Atkinson, 2004), excluding their consumption by other
166 oxidants (e.g., O_3). Thirteen experimental conditions were planned, covering the α-pinene,
167 isoprene and o-Cresol single precursor experiments (each at full, half and third reactivity)
168 respectively, binary α-pinene / isoprene, α-pinene / o-Cresol and o-Cresol / isoprene mixtures
169 and their ternary mixture. Initial concentrations of each VOC in the binary and ternary mixtures
170 were the same as the initial concentration in the half and third reactivity individual VOC
171 experiments respectively, ensuring comparable initial reactivity toward OH in all systems.

172

173 As described in Shao et al. (2022b), a "pre-experiment' program and a "post-experiment" were
174 conducted prior to and after each experiment. These two procedures consist of multiple auto
175 fill/flush cycle with high flow rate (~ 3 m^3 min^{-1}) with purified air to condition and remove the
176 unwanted contaminants in the chamber bag. A water condensation particle counter (WCPC;
177 TSI 3786), O_3 analyser, (Thermo Electron Corporation model 49C), NO-NO_2-NO_x analyser
178 (Thermo Electron Corporation model 42i) were used to monitor residual gas and particles in
179 the chamber during the "pre-experiment", to ensure their concentrations were close to zero in
180 the bag prior to chamber background procedure. The "chamber background" was conducted
181 for approximately 1h, while collection of data from the chamber in the dark, which the chamber
182 and all instrumentation are all stabilized. An "experimental background" procedure was
183 conducted in the next stage to establish the baseline contamination level in the chamber. This
184 comprised continuous measurement after injecting VOC(s), NO_x, and seed particles
185 sequentially and leaving the chamber to stabilise for an hour under dark condition. All the
186 subsequent analysis presented in this work has the "chamber background" and "experimental
187 background" subtracted. The baseline of clean background and the experimental background
188 were used to correct experimental data (See Supporting information Section 1). Actinometry
189 and off-gassing experiments were performed regularly during our campaign to monitor the
190 condition and cleanliness of the chamber bag.

191 The duration of each experiment was nominally 6 hours after initial illumination, under similar
192 controlled environmental conditions (RH:50±5% and T:24±2 ºC). The average OH
193 concentration during illumination was estimated from the decay rates of solely OH-reactive
194 VOCs (e.g., o-Cresol), yielding a concentration of approximately 1×10^6 molecules cm^{-3}. This

195 OH source arose from O_3 generated via NO_2 photolysis, which was further photolysed in the
196 moist chamber atmosphere. The summary of the initial conditions of the reported experiments
197 are presented in table 1 (noting the lack of third reactivity *o*-Cresol and half reactivity isoprene
198 owing to technical difficulties). To enhance confidence in the validity of our results and to
199 address technical issues caused by occasional instrument failures, repeat experiments were
200 conducted for selected single-precursor systems (both full and half reactivity), as well as for
201 the binary and ternary mixture systems. However, this study presents results from only one
202 experiment per system, with previous studies by Voliotis et al. (2021, 2022b) and Shao et al.
203 (2022a) already demonstrating good agreement across repeated experiments in terms of
204 maximum SOA mass, volatility distribution, and chemical composition within each system.
205 The particulate products were collected at the end of each experiment, flushing the entire
206 chamber contents through a pre-fired quartz filter (heating in a furnace at 550℃ for 5.5 hours),
207 which was subsequently wrapped in foil and refrigerated at -18 degrees.

208

209   Table 1: Summary of the initial conditions of experiments.

Exp. no.	Exp. Type	Precursors Reactivity	VOC	NO_x (ppb)	VOC (ppb)	VOC/ NO_x	Seed (µg m^{-3})
a		Full	α-pinene	40	309	7.7	72.6
b		Half	α-pinene	26	155	6.0	45.7
c		Third	α-pinene	18	103	5.7	51.0
d	**Single**	Full	*o*-Cresol	44	400	9.1	47.8
e		Half	*o*-Cresol	40	200	5.0	51.3
f		Full	isoprene	23	164	7.1	-
g		Third	isoprene	15	55	3.9	42.2
h		Full	*o*-cresol/isoprene	34	282 (200/82)	8.3	49.6
i	**Binary**	Full	α-pinene/*o*-Cresol	30	355 (155/200)	11.8	57
j		Full	α-pinene/isoprene	39	237 (155/82)	6.1	62.0
k	**Ternary**	Full	α-pinene/o-Cresol/isoprene	78	291 (103/133/55)	3.7	45.8

2.2. Instrumentation

2.2.1. Manchester Aerosol Chamber

All experiments were conducted in the Manchester Aerosol Chamber (MAC; Shao et al. (2022b). Briefly, the MAC operates as a batch reactor and consists of $18m^3$ volume Teflon FEP bag suspended by three rectangular extruded aluminium frames, housed in an air-conditioned enclosure. The enclosure is covered by reflective mylar material and is illuminated with two 6 kW Xenon arc lamps (XBO 6000 W/HSLA OFR, Osram) and a bank of halogen lamps (Solux 50 W/4700 K, Solux MR16, USA) with an intensity corresponding to a photolysis rate of NO_2 (jNO_2) around 1.83×10^{-3} s^{-1} through the entire experimental campaign. Conditioned air was introduced between the bag and the enclosure to maintain a constant chamber temperature throughout the experiment. Additionally, active water was used to cooling of the mounting bars of the halogen lamps and of the filter in front of the arc lamps to remove the unwanted heat from the lamps. Relative humidity (RH) and temperature (T) are controlled by the humidifier and by the air conditioning that couple with the chamber. RH and T were continuously monitored by the dewpoint hygrometer and several thermocouples and resistance probes during the experiment. Liquid VOCs (α-pinene, isoprene and o-cresol; Sigma Aldrich, GC grade $\geq$99.99% purity) were introduced into chamber through injection into a heated glass bulb for vaporization and subsequently flushed into the chamber with purified N_2 (electronic capture device-grade nitrogen stream; purity $\geq$99.998%). A custom-made cylinder (10% v/v) containing NO_x was used for NO_2 injection into the MAC in ECD N_2 as carrier gas. A Topaz model ATM 230 aerosol generator were used to produce ammonium sulphate seed particles by atomization from ammonium sulphate solution (Puratonic, 99.999% purity).

2.2.2. Online Measurement

The NO-NO$_2$-NO$_x$ and O$_3$ analysers were used to measure the NO_2 and O_3 gas concentration throughout the experiments. A semi-continuous gas chromatograph (6850 Agilent) coupled to a mass spectrometer (5975C Agilent; hereafter GC-MS) with a thermal desorption unit (Markes TT-24/7) was employed to monitor the time profile of VOC precursor decay. An Aerodyne high-resolution time-of-flight aerosol mass spectrometer (HR-ToF-AMS, Aerodyne Research Inc., USA) was used to measure organic mass loading and characterize the composition of non-

243   refractory organic particles. The HR-ToF-AMS instrument was calibrated by using

244   monodisperse (350nm) ammonium nitrate and ammonium sulphate particle prior to and after

245   to the experimental program, referring to the standard protocol in Jayne et al. (2000) and

246   Jimenez et al. (2003). The instrument operated in "V mode" during experiments and ran in

247   mass spectra (MS) and particle-time-of-flight (PToF) sub-modes for equal time periods (30s

248   each section). The HR-ToF-AMS data were processed in Igor Pro 7.08 (Wavemeterics.Inc.)

249   using the standard ToF-AMS analysis toolkit (version 1.21) for both unit mass resolution (UMR)

250   and high resolution (HR) analyses. The average ionisation efficiency of nitrate (IE=9.38×10^8),

251   the specific relative ionisation efficiencies (RIE) for NH_4^+ (3.57 ± 0.02) and SO_4^{2-} (1.28 ± 0.01)

252   from calibration, and the default RIE from Alfarra et al. (2004) of all organic compounds

253   (RIE=1.4) were all applied in the UMR and HR analysis. HR mass spectra was fitted using the

254   method of DeCarlo et al. (2006) and analysed using the ToF-AMS analysis software that

255   reported in Sueper et al. (2020). The ion fitting process for high resolution mass spectra in

256   our analysis refers to the supporting information in Hildebrandt et al. (2011), since this is

257   critical in the determination of the atomic ratio (O/C), and (H/C) of non-refractory organic

258   material.

259

260   The operation of the time-of-fight chemical ionisation mass spectrometer with iodide ionisation

261   coupled with a filter inlet for gases and aerosols (FIGAERO-CIMS ; Lopez-Hilfiker et al.

262   (2014)) was described in Voliotis et al. (2021). Briefly, the particles were sampled for 30 mins

263   to the PTFE filter (Zefluor, 2.0 μm pore size) at 1 sL min^{-1}, following by 33 mins thermal

264   desorption (15-min temperature ramp to 200 °C, 10 mins holding time and 8 mins

265   cooling down to room temperature) with ultra-high purity N_2 as carrier gas. The instrument

266   was run in negative-ion mode by producing I$^-$ regent ion generated using polonium-210

267   ionisation source to ionize methyl iodide (CH_3I). The I$^-$ reagent ions enter the ion molecule

268   reaction region (IMR) with N_2 (ultra-high purity) as carrier gas. An "instrument background"

269   procedure for the particle phase measurements was conducted in all the experiments for

270   subtraction from the measurements. The FIGAERO-CIMS data were processed by using the

271   Tofware package in Igor Pro 7.0.8 (version. 3.2.1., Wavemetrics©) (Stark et al., 2015) for peak

272   identification. A data set of assigned molecular formula of detected compounds were produced,

273   allowing subsequent determination of the H/C and O/C ratios.

274

2.2.3. Offline Measurement

Ultra-performance liquid chromatography ultra-high resolution mass spectrometry (Dionex 3000, Orbitrap QExactive, ThermoFisher Scientific) was employed for analysing the filter sampled particulate. A detailed description of the instruments, experimental set-up and data processing methodology can be found on Shao et al. (2022a) and Pereira et al. (2021). Briefly, the preparation of sample solution is as follows:

1) Filter samples were dissolved in 4 mL of LCMS-grade methanol, left to stand for 2 hours at ambient temperature, and then extracted using sonication for 30 minutes (Fisher Scientific FB15051).

2) 0.22 μm pore size PDVF filter (Fisher Scientific) and BD PlasticPak syringe (Fisher Scientific) were used for filtering the sample solution, followed by adding further 1 ml methanol on the dry filter for the second extraction of samples with the same method.

3) The extracted solution was evaporated to dryness using a solvent evaporator (Biotage) under specified temperature (36 °C) and pressure (8 mbar) conditions. The evaporation step may result in the partial loss of the most volatile SOA components; however, most LCMS detectable species are of low-volatility and thus retained under these conditions.

4) The extract residual was re-dissolved in 1 ml solvent that consists of LCMS optimal grade water and methanol in a ratio of 9:1.

Once the sample solutions were prepared, they were injected into the UHPLC-HRMS 0.3 ml/min with 2 μl volume by autosampler held at 4 °C. The mass spectrometer was mass calibrated using ESI positive and negative ion calibration solutions (Pierce, Thermo Scientific) prior to sample analysis. The sample solution was passed through a reverse-phase C18 column (Accucore, Thermo Fisher Scientific) 100 mm long × 2.1 mm wide and with 2.6 μm particle size, with temperature held at 40°C. The mobile phase was composed of (A) LCMS optimal grade water (Sigma Aldrich) and (B) methanol (LC-MS Optimal grade, Fisher Scientific) that both contain 0.1% (v/v) formic acid (Sigma Aldrich, 99% purity). The gradient elution started at 90% (A) with a 1-minute post-injection hold, decreased to 10% (A) over 26 minutes, returned to the initial mobile phase at 28 minutes, and ended with a 2-minute re-equilibration In this

306 instrument, electrospray ionisation (ESI, 35 eV) was performed for both positive and negative

307 mode to charge the organic compounds in a range of m/z 80 to m/z 750. High-energy

308 collisional dissociation from tandem mass spectrometry (MS^2) was used to generate ion

309 fragments for subsequent mass analyser detection. The resulting product ion spectra were then

310 used to support structural characterisation and isomer identification of the compounds.

311 Analysis of extracted solvent (water: methanol = 9:1) and pre-conditioned bank filter was also

312 performed with the same procedure for subtraction from the measurements to ensure exclusion

313 of baseline noise and artefacts from sample preparation.

314 The data was processed by an automated methodology for non-targeted composition of small

315 molecules (Pereira et al. (2021). This approach guided the peak identification and molecular

316 formula assignment for detected compounds, enabling calculation of the signal weighted $\overline{OSc}$,

317 O/C , H/C and H/C for each system.

318

319

2.3. Estimation of average carbon oxidation state ($\overline{OSc}$)

321

322 For compounds that contain only carbon, hydrogen and oxygen (designated "CHO"

323 compounds), the average $\overline{OSc}$ was straightforwardly determined using atomic ratios O/C and

324 H/C using equation 1, $\overline{OSc}$= 2*O/C-H/C, in analysis of data from all MS techniques.

325 For compounds that additionally contain nitrogen ("CHON" compounds), it is assumed that

326 the nitrogen would exist as nitrate with $\overline{OS_N} = +5$ if there are 3 or more oxygen atoms in the

327 molecule and as nitrite with $\overline{OS_N} = +3$ if there are fewer than 3 oxygen atoms. For CHON

328 compounds, the $\overline{OSc}$ is therefore calculated using equation (2) where the H, C, O and N are

329 determined from the FIGAERO-CIMS and UHPLC-HRMS signal.

330 $$\overline{OSc} = 2 * \frac{O}{C} - \frac{H}{C} - \left(\overline{OS_N} * \frac{N}{C}\right) \hspace{2cm} (2)$$

331 Where N/C corresponding to nitrogen-to-carbon ratios, $\overline{OS_N}$= 3 if nO < 3; or $\overline{OS_N}$ = 5 if nO ≥

332 3. The signal-weighted average $\overline{OSc}$ determined by equation (2) will be presented in section 3

333 and referred to as "accounting for $\overline{OS_N}$". The HR-ToF-MS is unable to provide molecular

334 information, but provides total particle ensemble C, H and O from the HR mass defect.

335 However, retrieval of mass defect with sufficient accuracy to attribute the N-containing

336 compounds at the resolution of the instrument is too challenging to be considered robust. The

calculated $\overline{OSc}$ from HR-ToF-AMS data uses only C, H and O and uses equation 1 (i.e. implicitly not accounting for organic nitrogen in any CHON compounds present). For comparison with the HR-ToF-AMS -calculated $\overline{OSc}$, the average $\overline{OSc}$ for CHON compounds measured by the FIGAERO-CIMS and UHPLC-HRMS technique has also been calculated ignoring the N and using equation (1), and this referred to as "not accounting for $\overline{OS_N}$". in section 3

Strictly, the estimation of average carbon oxidation state should account for the oxidation state of sulphur $(\overline{OSs})$ in any sulphur-containing compounds (CHOS and CHONS compounds) in the particles. Given the challenges associated with the quantification of S-containing compounds in FIGAERO-CIMS technique (Xu et al., 2016; D'ambro et al., 2019), this study does not consider the contribution of $\overline{OSs}$ in $\overline{OSc}$ calculation. It was also shown by Du et al. (2021) that the influence of heteroatom S or NS on $\overline{OSc}$ calculation would be negligible as a result of their low fractional abundance the in UHPLC-HRMS measurements (see also Shao et al. 2022a).

In this study, the average $\overline{OSc}$ reported from a "representative experiment," where only the compounds found in all replicate experiments can be confidently attributed to this particular system in both UHPLC-HRMS and FIGAERO-CIMS analyses. The HR-ToF-AMS measurements were selected from the same 'representative experiment' as the UHPLC-HRMS and FIGAERO-CIMS analyses.

3. Result
3.1. 3.1. Average $\overline{OSc}$ Evolution of single precursor experiments (with $\overline{OS_N}$ correction)

Figure 1 shows the average $\overline{OSc}$ as a function of SOA mass concentration from single α-pinene and *o*-Cresol experiments with different initial reactivities respectively, derived from FIGAERO-CIMS and UHPLC-HRMS measurements. All values shown here include the $\overline{OS_N}$ correction.

367   For the single α-pinene system (Fig. 1a), the average $\overline{OSc}$ estimated from FIGAERO-CIMS

368   decreased with increasing SOA mass across all three reactivity levels. The magnitude of this

369   decrease was similar among experiments. In the third reactivity experiment (lowest precursor

370   concentration), the average $\overline{OSc}$ declined from −0.24 to −0.46, while in the half reactivity

371   experiment it decreased from −0.31 to −0.51, and in the full reactivity experiment from −0.35

372   to −0.57.

373   The UHPLC-HRMS results in negative ionisation mode showing comparable trends. In

374   negative ionisation mode, the endpoint average $\overline{OSc}$ values were −0.45 for the third reactivity

375   α-pinene experiment, which is higher than that a half reactivity ($\overline{OSc}$ = -0.61) and full

376   reactivity ($\overline{OSc}$ = -0.58) experiment. In positive ionisation mode, the half and full reactivity

377   experiments gave similar average $\overline{OSc}$ magnitude (around −0.95), which were about 0.26

378   higher than the third reactivity experiment.

379   For the *o*-Cresol system (Fig. 1b), the average $\overline{OSc}$ from FIGAERO-CIMS decreased with

380   increasing SOA mass in both reactivity experiments. In the full reactivity experiment, the

381   average $\overline{OSc}$ declined from 0.12 to −0.26, while in the half reactivity experiment it decreased

382   from 0.09 to −0.37. At the very beginning of the half reactivity experiment, the first point shows

383   a lower $\overline{OSc}$ of about −0.25, but this corresponds to exceptionally low SOA mass loadings.

384   The UHPLC-HRMS results show similar behaviour. In negative ionisation mode, the full and

385   half reactivity experiments gave comparable endpoint values of around −0.55. In positive

386   ionisation mode, however, the half-reactivity experiment has a higher $\overline{OSc}$ (−0.48) than the

387   full reactivity experiment (−0.66).

388
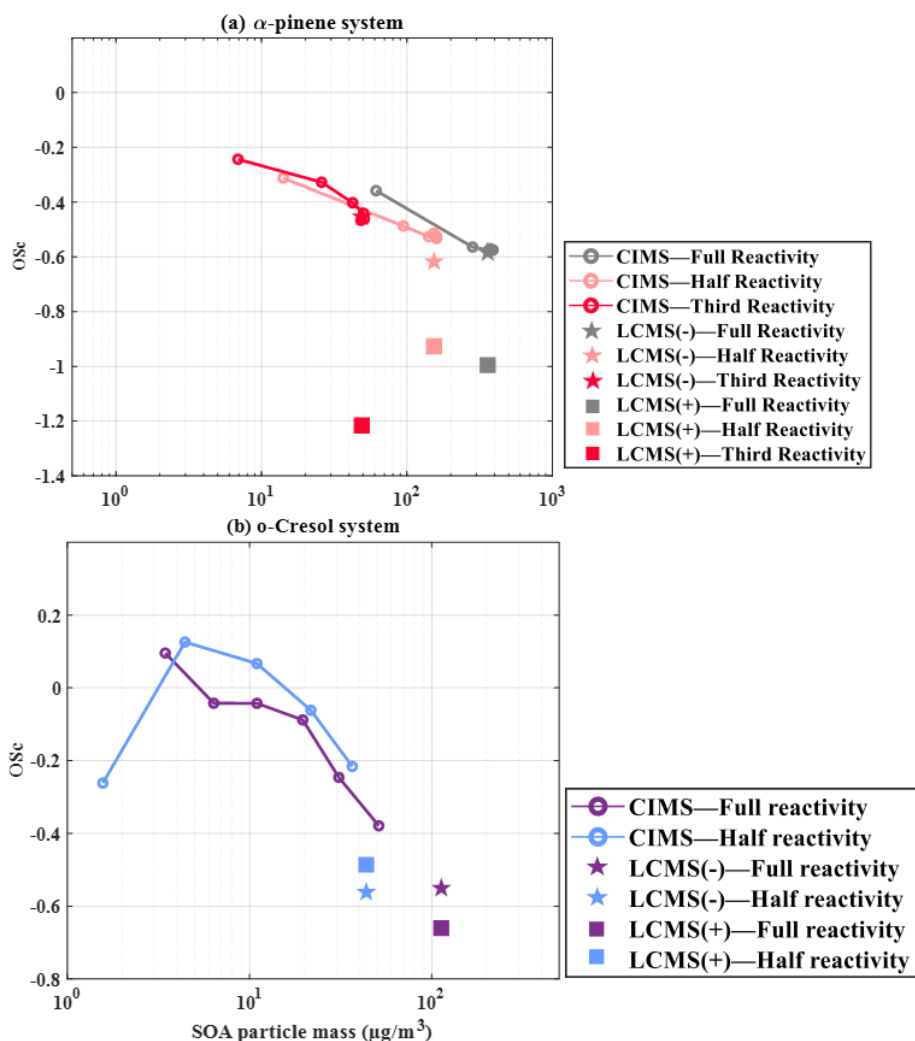
Figure 1 : Average $\overline{OSc}$ (with $\overline{OS_N}$ correction) estimated from the FIGAERO-CIMS (Lines) and UHPLC-HRMS (symbols; negative ion mode = stars, positive ion mode = squares) as a function of SOA mass. (a) Single a-pinene experiments with three initial reactivity: (b) Single *o*-Cresol experiments with two initial reactivity

3.2.   Average $\overline{OSc}$ Evolution of single precursor experiments (without $\overline{OS_N}$ correction)

Figure 2 shows the evolution of $\overline{OSc}$ as a function of SOA mass in single α-pinene and *o*-Cresol experiments across different reactivities, estimated using HR-ToF-AMS, FIGAERO-CIMS, and UHPLC-HRMS measurement. It is important to note that the average $\overline{OSc}$ value in Figure 2 do not include the $\overline{OS_N}$ correction term.

402   In the single α-pinene experiments (Fig. 2a), the HR-ToF-AMS is able to estimate $\overline{OSc}$ at

403   lower particle mass during the rapid early growth phase compared with the other two

404   techniques. The half reactivity experiment exhibits the highest average $\overline{OSc}$ (-1 to -0.5),

405   followed by the by the full reactivity experiment ($\overline{OSc}$: -1.6 to -0.7) while the third reactivity

406   experiment remains lowest ($\overline{OSc}$: -2.48 to -0.68). In both the full and half reactivity

407   experiments, the average $\overline{OSc}$ initially increases and then declines as SOA mass builds,

408   whereas in the third reactivity experiment it increases continuously until the end of the

409   experiment. By contrast, FIGAERO-CIMS consistently reports higher $\overline{OSc}$ than the AMS

410   across all three experiments. For FIGAERO-CIMS, the full ($\overline{OSc}$: –0.17 to –0.40) and half

411   reactivity ($\overline{OSc}$: –0.17 to –0.32) experiments give comparable values, both slightly lower than

412   the third reactivity experiment ($\overline{OSc}$: –0.07 to –0.22), which is the opposite trend to that

413   observed with AMS measurement. The UHPLC-HRMS results also align more closely with

414   FIGAERO-CIMS, with the third reactivity experiment giving $\overline{OSc}$ of –0.34 in negative

415   ionisation mode and –0.19 in positive ionisation mode, with the negative ionisation values all

416   comparable to the FIGAERO-CIMS estimates.

417

418   For the single o-Cresol experiments, the HR-ToF-AMS derived average $\overline{OSc}$ shows a broadly

419   increasing trend with SOA mass under both full and half reactivity conditions, with magnitudes

420   ranging from -1.2 to 0.2 (Fig. 2b). The two experiments are generally comparable, except that

421   the full reactivity experiment exhibits a slight decline in average $\overline{OSc}$ once SOA mass peaks

422   at ~10 μg m⁻³. In addition, FIGAERO-CIMS estimation showed higher average $\overline{OSc}$ than HR-

423   ToF-AMS measurement, with comparable values between the two reactivity conditions, and a

424   clear decrease from ~0.4 to ~0 as particle mass increases. The UHPLC-HRMS measurements

425   also show similar behaviour across reactivities. In negative ionisation mode, the average $\overline{OSc}$

426   is ~0.14 in both experiments, while in positive mode the full reactivity experiment gives –0.36,

427   about 0.11 lower than the half reactivity experiment.

428
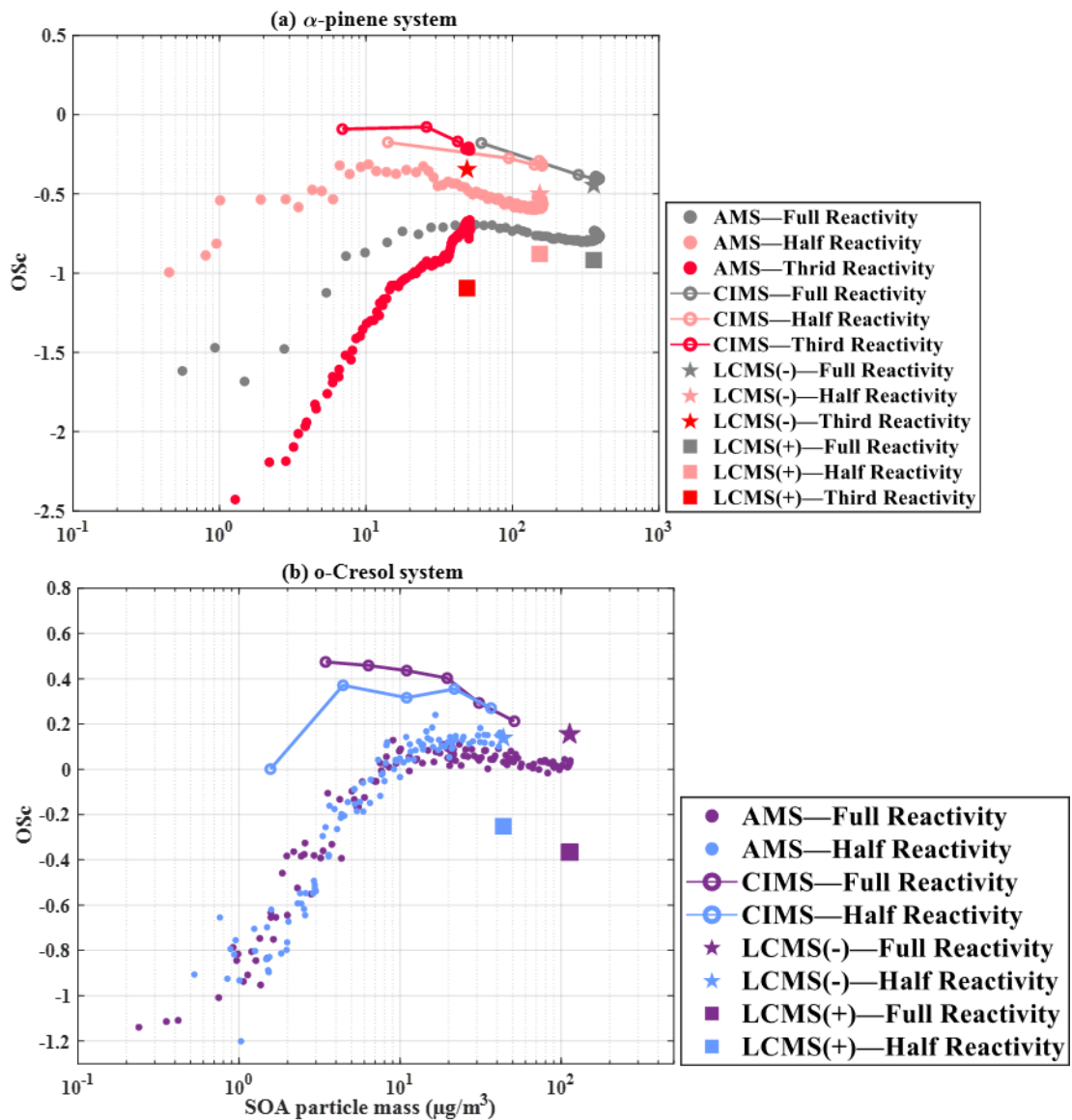
Figure 2. Average $\overline{OSc}$ (without $\overline{OS_N}$ correction) as a function of SOA particle mass for single-precursor systems: (a) α-pinene with three initial reactivity and (b) o-Cresol with two initial reactivity, obtained from HR-ToF-AMS (Dots), FIGAERO-CIMS (Lines), and UHPLC-HRMS (symbols; negative ion mode = stars, positive ion mode = squares).

3.3. Average $\overline{OSc}$ Evolution in mixed precursor system (with $\overline{OS_N}$ correction)

Figure 3 illustrated that the average $\overline{OSc}$ evolution as a function of SOA mass concentration from mixture precursor system along with their reference single experiments, obtained from

 FIGAERO-CIMS and UHPLC-HRMS measurements. All values shown here include the $\overline{OS_N}$

441   correction.

(a) α-pinene/Isoprene binary system

443   Figure 3a shows that the average $\overline{OSc}$ in the half reactivity α-pinene experiment exhibits a

444   declining trend (–0.31 to –0.51) similar to that observed in the α-pinene/isoprene binary

445   mixture ($\overline{OSc}$: –0.42 to –0.65), based on FIGAERO-CIMS measurements. For comparison, we

446   also include the single full reactivity isoprene experiment as a reference, noting that the single

447   half reactivity isoprene experiments were not available. In the single isoprene experiment, SOA

448   mass concentrations were negligible (<1 μg m^{-3}, close to chamber background), while the

449   corresponding average $\overline{OSc}$ remained between –0.2 and 0.4.

450   The UHPLC-HRMS results demonstrated comparable average $\overline{OSc}$ in negative ionisation

451   mode between the binary mixture and the single α-pinene experiment (and aligns with the

452   FIGAERO-CIMS endpoints at $\overline{OSc} \approx$–0.6). In positive ionisation mode, however, the single

453   full reactivity α-pinene experiment shows a slightly higher $\overline{OSc}$ than the mixture ($\overline{OSc} \approx$–

454   0.92) (Fig. 3a).

455

(b) *o*-Cresol/Isoprene binary system

457   From FIGAERO-CIMS measurement, both the binary *o*-Cresol/Isoprene and the single *o*-

458   Cresol experiment display a decrease in average $\overline{OSc}$ with increasing SOA mass beyond ~3

459   μg m^{-3} as shown in Figure 3b. In the binary mixture system, the average $\overline{OSc}$ declines from

460   0.38 at 3 μg m^{-3} to –0.21 by the end of the experiment. For the single *o*-Cresol run, the average

461    $\overline{OSc}$ starts around –0.25 during the initial low mass period (<3 μg m^{-3}, roughly the first hour),

462   then decreases more modestly from 0.12 to –0.26 as SOA mass increases (Fig. 3b). For

463   reference, results from single isoprene experiments are also shown in Figure 3b. However, the

464   SOA mass concentrations were close to chamber background, so their average $\overline{OSc}$ estimates

465   should be interpreted with caution.

466   In the UHPLC-HRMS measurements, the positive ionisation mode has comparable average

467    $\overline{OSc}$ values for the binary mixture and single *o*-Cresol systems ($\approx$ –0.50). In contrast, the

468   negative ionisation mode shows slightly higher average $\overline{OSc}$ in the single *o*-Cresol

469   experiment ($\approx$ –0.55) than in the binary mixture ($\approx$ –0.71) (Fig. 3b).

470

(c) *o*-Cresol/α-pinene binary system

Figure 3c shows that the FIGAERO-CIMS average $\overline{OSc}$ decreases with SOA mass concentration above ~3 µg m^{-3} in the binary *o*-Cresol/α-pinene system as well as in the single half reactivity *o*-Cresol and α-pinene experiments. In the binary mixture system, the average $\overline{OSc}$ declines from 0.09 to –0.34, a change comparable to that observed in the single half reactivity *o*-Cresol experiment (0.12 to –0.26), but larger than in the single half reactivity α-pinene experiment (–0.31 to –0.51).

In negative ionisation mode of UHPLC-HRMS measurement, the binary mixture has an average $\overline{OSc}$ of –0.63, in reasonable agreement with the single half reactivity α-pinene experiment. By contrast, in positive ionisation mode, the binary mixture produces a substantially lower average $\overline{OSc}$ ($\approx$ –1.38) than either of the single precursors experiment, which were $\approx$ –0.50 for *o*-Cresol and $\approx$ –0.92 for α-pinene.

(d) α-pinene/Isoprene/*o*-Cresol ternary system

Figure 3d shows that the average $\overline{OSc}$ exhibits a declining trend with increasing SOA mass in the ternary mixture system as well as in all single precursor experiments. In the ternary mixture system, the FIGAERO-CIMS average $\overline{OSc}$ decreases from –0.16 to –0.35, falling between the single third reactivity α-pinene experiment ($\overline{OSc}$: –0.24 to –0.26) and the half reactivity *o*-Cresol experiment ($\overline{OSc}$: 0.10 to –0.21, excluding the first hour when SOA mass was very low). This suggests contributions from both precursors. It is noting that data for the third reactivity *o*-Cresol experiment were not available due to instrument failure. For isoprene, the single third reactivity experiment produced only ~2 µg m^{-3} of measurable SOA mass. In this case, the average $\overline{OSc}$ estimated by FIGAERO-CIMS decreased sharply from ~1 to –0.5.

The UHPLC-HRMS results show that in negative ionisation mode, the ternary mixture system has an average $\overline{OSc}$ comparable to the single half reactivity *o*-Cresol experiment ($\overline{OSc} \approx$ –0.55), but slightly lower than the single third reactivity α-pinene experiment ($\overline{OSc} \approx$ –0.45). By contrast, in positive ionisation mode the ternary mixture has an average $\overline{OSc}$ similar to the single third reactivity α-pinene experiment ($\overline{OSc} \approx$ –1.2) but much lower than the single half reactivity *o*-Cresol experiment ($\overline{OSc} \approx$ –0.48).
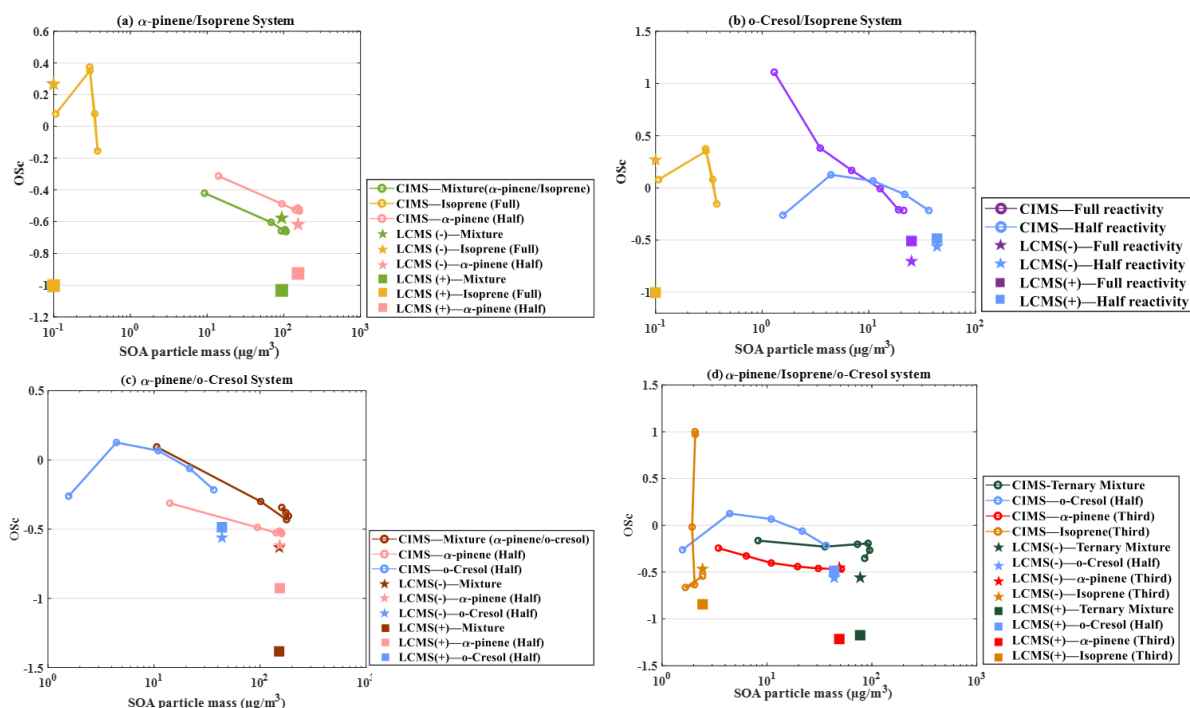
Figure 3. Evolution of the average $\overline{OSc}$ (with $\overline{OS_N}$ correction) as a function of SOA mass concentration for binary and ternary precursor systems, compared with the corresponding single precursor reference experiments. Results are shown from FIGAERO-CIMS (lines) and UHPLC-HRMS (symbols; negative ion mode = stars, positive ion mode = squares). Panels show (a) α-pinene/ isoprene mixture, (b) *o*-Cresol /isoprene mixture, (c) α-pinene/*o*-Cresol mixture, and (d) ternary α-pinene + *o*-Cresol + isoprene system.

4. Discussion

4.1. Average $\overline{OSc}$ Evolution with SOA Mass and Implication for Volatility and SOA Aging

The evolution of average $\overline{OSc}$ that estimated accounting for the $\overline{OS_N}$ term as a function of SOA mass could provide insight into the underlying chemical processes of SOA formation and aging. In the single α-pinene and *o*-cresol experiments across all initial reactivities (Figs. 1), $\overline{OSc}$ estimated from FIGAERO-CIMS measurements generally shows a declining trend as SOA mass increases. This behaviour suggested an increasing contribution from less oxidised material as particulate matters loading builds. It is possible that SOA growth is dominated by highly oxygenated, low-volatility products, likely formed via functionalisation of the precursor at the early stage. As SOA mass accumulates, the absorptive capacity of the particles increases, allowing semi-volatile, less oxidised compounds to partition, thereby driving down the bulk average $\overline{OSc}$. This interpretation is supported by the companion study of Voliotis et al. (2021),

521 which reported pronounced fragmentation and a higher fraction of more-volatile product in the

522 single α-pinene system, that such species could contribute at later stages once sufficient mass

523 has accumulated.

524 Importantly, this relationship between average $\overline{OSc}$ and SOA mass is consistent across

525 different initial precursor concentrations. In the single α-pinene experiments, all three reactivity

526 levels (full, half, third) follow the same qualitative decline, showing that the observed

527 behaviour is robust to starting conditions. For single o-Cresol experiments, the half reactivity

528 experiment begins with lower average $\overline{OSc}$ than the full reactivity experiment, but once the

529 SOA mass reaches to comparable level, the two converge and decline together. This

530 demonstrates that average $\overline{OSc}$ evolution is primarily controlled by the partitioning balance

531 during particle growth rather than the absolute precursor concentration.

532 The estimated average $\overline{OSc}$ from UHPLC-HRMS (accounting for the $\overline{OS_N}$, term) across the

533 three α-pinene experiments show small differences, but the $\overline{OSc}$ in negative ionisation mode

534 is consistently higher than in positive ionisation mode. A plausible explanation is that the

535 negative ionisation mode preferentially detects deprotonated acids and highly oxygenated

536 compounds (e.g. carboxylic acids) whereas the positive ionisation mode favours compounds

537 with readily protonated functional groups, typically less acidic and less oxidised species. The

538 negative ionisation mode $\overline{OSc}$ also aligns closely with the FIGAERO-CIMS endpoint values,

539 likely because both techniques are more sensitive to highly oxygenated, low-volatility species,

540 and therefore capture a similar subset of the SOA composition. For the single o-Cresol system,

541 the average $\overline{OSc}$ in negative ionisation mode are comparable between the full and half

542 reactivity experiments, that mainly contributed by nitro-aromatic molecules, which is dominate

543 products in o-Cresol oxidation and to be sensitively detected in negative ionisation mode (Shao

544 et al; 2022a). On the other hand, the positive ionisation mode average $\overline{OSc}$ in half reactivity

545 experiment is higher than full reactivity experiment, suggesting that the latter may contain a

546 larger fraction of less-oxidised neutral species and oligomeric condensation products.

547

548

549 ## 4.2. Influence of precursor mixture on average $\overline{OSc}$ during SOA formation

550 While the metric $\overline{OSc}$ in single volatile precursor systems has been considered, its application

551 to SOA formed from mixtures of VOCs remains limited. Yet, in the real atmosphere, SOA

552 almost always derives from multiple precursors undergoing simultaneous reactions. Examining

553 how mixtures alter $\overline{OSc}$ trends compared with single precursor experiment could offers novel

554 insight into whether additional or modified chemical processes emerge when different VOCs

555 simultaneous reacted. Beyond identifying these mechanistic differences, such comparisons

556 provide useful constraints for future modelling efforts that aim to represent the chemical

557 complexity of ambient SOA. To support this evaluation, this study presents the trend of

558 average $\overline{OSc}$ (account for $\overline{OS_N}$ *N/C correction term) driven from FIGAERO-CIMS and

559 UHPLC-HRMS, shown as function of increasing SOA particle mass in binary and ternary

560 mixture precursor mixture system, and compared against the corresponding single precursor

561 reference experiments. Corresponding O:C, H:C, and N:C ratios for each mixture system are

562 shown in the Supporting Information (Figs. S2-S5) to provide additional detail underlying the

563 average $\overline{OSc}$ evolution.

564

565 **(a) α-pinene/Isoprene binary system**

566 According to FIGAERO-CIMS measurement, both the α-pinene/isoprene mixture system and

567 the single half reactivity α-pinene experiment show decreasing average $\overline{OSc}$ with increasing

568 SOA mass (Fig. 3a). However, the binary system is consistently offset to slightly lower $\overline{OSc}$

569 at comparable mass loadings, likely reflecting suppression of highly oxygenated α-pinene

570 products by isoprene (via RO_2 competition and reduced HOM formation) and a larger relative

571 contribution of less oxidised condensable molecules as the aerosol grows. Isoprene oxidation

572 with OH radicals primarily produce semi-volatile C_4–C_5 species with high volatility (e.g.

573 hydroxycarbonyls), which could suppress α-pinene SOA yields in mixed systems (Wennberg

574 et al., 2018; Stroud et al., 2001; Carlton et al., 2009). An alternative interpretation is that these

575 semi-volatile isoprene products partition onto the growing α-pinene driven particle phase,

576 lowering the average $\overline{OSc}$ of the mixture. This interpretation is consistent with the findings of

577 Voliotis et al. (2022a), where isoprene driven products accounted for ~3% of the total

578 FIGAERO-CIMS signal in the binary system. Moreover, comparison across experiments

579 indicates higher N/C ratios in the binary system than in the single half reactivity α-pinene

580 experiment (See Fig. S2(c)), suggesting that the presence of isoprene enhances the contribution

581 of CHON species, which further drives down the average $\overline{OSc}$ in the mixed system.

582 The UHPLC-HRMS results fairly agree with these trends (Fig.3a). In negative ionisation mode,

583 the mixed system has slightly higher average $\overline{OSc}$ than the single half reactivity α-pinene

584   experiment, likely reflecting additional condensable acidic or highly oxygenated products from

585   isoprene that are preferentially detected in negative ionisation mode. By contrast, in positive

586   ionisation mode the binary system shows a slightly lower average $\overline{OSc}$ than the single half

587   reactivity α-pinene experiment, which suggested the partitioning balance might shifts toward

588   less oxidised semi-volatile or oligomeric species when isoprene is present.

589

590   **(b) *o*-Cresol/Isoprene binary system**

591   The binary *o*-Cresol/isoprene system shows an average $\overline{OSc}$ evolution that can be described

592   in two stages based on the FIGAERO-CIMS data. At the beginning of the experiment, when

593   SOA mass was exceptionally low in both the binary and the single half reactivity *o*-Cresol

594   system, the mixture exhibits a substantially higher average $\overline{OSc}$.(Fig. 3b). This might suggest

595   the formation of highly oxygenated accretion products when isoprene is present. Such HOM

596   like species may arise from RO_2 cross reactions between isoprene and *o*-Cresol driven radicals,

597   as well as from nitroaromatic compounds formed under NOx conditions. Although these

598   species likely represent only a small fraction of the particle mass, their high oxygen content

599   can disproportionately elevate the average $\overline{OSc}$ at early stage of experiment.

600   The average $\overline{OSc}$ declines as SOA mass increases, that likely reflecting isoprene acts as an

601   OH scavenger in the binary mixture system. This reduces the OH available for *o*-Cresol

602   oxidation and suppresses the formation of highly oxidised *o*-Cresol products. Generally, *o*-

603   Cresol RO_2 radicals generated via OH addition undergo autoxidation to form HOMs, but in the

604   mixture these pathways potentially curtailed by competition with isoprene driven RO_2 and NOx.

605   Instead of HOMs formation, the chemistry is likely diverted toward accretion or fragmentation

606   channels, producing less oxidised products. This shift could reduce the contribution of highly

607   oxygenated *o*-Cresol products, explaining why the binary mixture system evolves toward lower

608   average $\overline{OSc}$ than the single half reactivity *o*-Cresol experiment at higher SOA mass.

609   In the UHPLC-HRMS measurements, the positive ionisation mode has comparable average

610    $\overline{OSc}$ values for both the single half reactivity *o*-Cresol and the binary *o*-Cresol/isoprene

611   experiments (Fig. 3b), suggesting that both systems may generate a similar contribution of less

612   acidic or neutral compounds. In contrast, the negative ionisation mode has higher average $\overline{OSc}$

613   in the single half reactivity *o*-Cresol experiment compared with the binary mixture system. This

614   likely reflects a relatively less contribution of CHON compounds in the single half reactivity

615   *o*-Cresol experiment compared to the mixture system, as the negative ionisation mode is

616   particularly sensitive to nitroaromatic species that dominate the CHON class. These nitrogen-

617   containing oxygenated compounds could affect the $\overline{OS_N}$ correction term, leading to lower

618   average $\overline{OSc}$ values when they are abundant. Previous work has shown that CHON

619   compounds dominate o-Cresol SOA (>95% of the signal in both single and binary systems;

620   Shao et al., 2022a), even though those results were obtained under full reactivity conditions.

621   This observation still highlights the influence of CHON species in average $\overline{OSc}$ estimation

622   and reminds the importance of SOA chemical composition as well as by the compound classes

623   to which each instrument is most sensitive.

624

625   **(c) α-pinene/*o*-Cresol binary system**

626   The average $\overline{OSc}$ in the α-pinene/o-cresol binary system decreases as SOA mass grows that

627   estimated from FIGAERO-CIMS measurement. At the early stage, the mixture exhibits

628   average $\overline{OSc}$ comparable to the single half reactivity *o*-Cresol experiment but consistently

629   higher than the single half reactivity α-pinene experiment at overlapping SOA mass (Fig.3c).

630   One possible explanation is that FIGAERO-CIMS has high sensitivity to nitroaromatic

631   products generated from *o*-Cresol oxidation (Voliotis et al. (2021), so the binary mixture system

632   is weighted toward these highly oxygenated aromatic products. This sensitivity likely explains

633   why the binary mixture system shows a similar magnitude of average $\overline{OSc}$ to the single half

634   reactivity *o*-Cresol experiment, despite α-pinene being the higher SOA yield precursor. Toward

635   the end of the experiment, the SOA mass of the binary mixture approaches that of the single

636   half reactivity α-pinene experiment, but its average $\overline{OSc}$ remains higher, that might be

637   attributed by the formation of additional multifunctional, low-volatility products via cross

638   reactions between α-pinene and o-Cresol driven RO_2 radicals.

639   Interestingly, this behaviour is not consistent as the *o*-Cresol/isoprene binary system, where the

640   mixture evolved to lower average $\overline{OSc}$ than the single precursor experiment at the end of the

641   experiment. The difference can be explained by isoprene driven RO_2 (highly volatile)

642   suppresses the formation of highly oxygenated *o*-Cresol products, lowering the average $\overline{OSc}$

643   as the SOA mass increased. whereas α-pinene driven semi-volatile RO_2 favours the formation

644   of multifunctional oxygenated accretion products that elevate the average $\overline{OSc}$ of binary

645   mixture system. Moreover, α-pinene does not act as a strong OH scavenger compared with

646   isoprene according to their reactivity (Dillon et al., 2017), so *o*-Cresol oxidation by OH might

647   partly retained, and autoxidation of *o*-Cresol driven RO₂ may still proceed to form low
648   volatility oxygenated dimers.

649   The binary mixture system shows a slightly lower average $\overline{OSc}$ than the single *o*-Cresol
650   experiment in negative ionisation mode of UHPLC-HRMS measurement (Fig.3c). From the
651   accompanying atomic ratios (See Fig.S4), this is driven by lower O:C and higher H:C ratio in
652   the mixed precursor system, while N/C is comparable or smaller, which could explain that the
653   difference is not due to a larger nitrogen containing compounds correction. In contrast, the
654   average $\overline{OSc}$ in the binary mixture is substantially lower than in either single precursor
655   experiment in positive ionisation mode (Fig. 3c). This likely reflects a greater contribution of
656   less acidic, lower O/C neutral species and oligomers produced through cross interactions in the
657   binary mixture system compared to both single precursor experiment, which are preferentially
658   detected in positive ionisation mode.

659

660   **(d) Ternary system**

661   The average $\overline{OSc}$ in the ternary α-pinene/*o*-Cresol/isoprene system decreases as SOA mass
662   builds up (Fig. 3d) based on FIGAERO-CIMS measurement. Within the overlapping SOA mass
663   range, the mixture sits between the single third reactivity α-pinene and single half reactivity *o*-
664   Cresol experiments, being higher than the α-pinene experiment but lower than the *o*-Cresol
665   experiment. This behaviour may suggest several competing chemical processes involve in the
666   ternary mixture system rather than one dominate mechanism. For example, isoprene can act as
667   an OH scavenger, slowing the multigenerational oxidation of α-pinene and *o*-Cresol, and
668   thereby suppressing the formation of highly oxygenated products. The presence of isoprene
669   may also enhance the RO₂+NO reaction, diverting chemistry toward organonitrates and
670   fragmentation products, while limiting RO₂ + HO₂ pathways that typically drive
671   functionalisation and higher average $\overline{OSc}$. Also, cross interactions between *o*-Cresol driven
672   RO₂ and α-pinene or isoprene driven RO₂ could further suppress autoxidation of *o*-Cresol
673   precursor, with consequences for both O/C and N/C atomic ratio. These effects together may
674   explain why the ternary system evolves to intermediate $\overline{OSc}$ values, but the relative
675   importance of each pathway remains unclear.

676   The UHPLC-HRMS negative ionisation mode reported the average $\overline{OSc}$ in the ternary mixture
677   system is comparable to the single half-reactivity *o*-Cresol experiment, but slightly lower than
678   the single third reactivity α-pinene system (Fig. 3d). This suggests that nitroaromatic and other

679 highly oxygenated CHON species, mainly characteristic of o-Cresol oxidation, remain an
680 important contribution within the mixture system. In contrast, the positive ionisation mode
681 indicates that the ternary mixture system aligns more closely with the single α-pinene
682 experiment. This points to a strong influence of neutral and oligomeric products in the ternary
683 mixture system, likely including accretion products formed through cross-interactions between
684 precursors.

685

4.3. Average $\overline{OSc}$ Comparison across three Mass Spectrometry Techniques

688 Although $\overline{OSc}$ is widely used as a metric to characterise SOA, its estimation depends strongly
689 on the measurement technique. In this study, we shown a comparison across HR-ToF-AMS,
690 FIAGERO-CIMS, and UHPLC-HRMS, to illustrate how instrumental properties impact the
691 $\overline{OSc}$ estimation of SOA particles. The combination of online and offline mass spectrometric
692 techniques to estimate average $\overline{OSc}$ has not been widely adopted, particularly in mixed
693 precursor chamber studies.

694 From Fig.2, the FIGAEREO-CIMS reported higher estimated average $\overline{OSc}$ (not accounting
695 for $\overline{OS_N}$) compared to the UHPLC-HRMS and HR-ToF-AMS values in α-pinene and o-
696 Cresol experiments across all initial reactivities, that likely due to its strong sensitivity toward
697 highly oxygenated (Lee et al., 2014), low volatility compounds and the potential contribution
698 of thermal decomposition fragments (Du et al., 2021). Moreover, the averaged $\overline{OSc}$ in
699 UHPLC-HRMS negative ionisation mode broadly agree with the FIGAERO-CIMS endpoint
700 values, which might reflect their shared bias toward acidic and highly oxygenated compounds,
701 whereas the positive ionisation mode more favour to detect the less oxidised neutral or
702 oligomeric species leading to have lower average $\overline{OSc}$. The HR-ToF-AMS has average $\overline{OSc}$
703 estimation generally lower than FIGAERO-CIMS but higher than positive ionisation mode of
704 UHPLC-HRMS (Fig.2). For single α-pinene experiments, HR-ToF- AMS has similar decline
705 trend as the FIGAERO-CIMS in average $\overline{OSc}$ in the full and half reactivity experiments but
706 diverges in the third reactivity experiment, while for o-Cresol the HR-ToF-AMS reports an
707 initial rise and then reach to a plateau. These discrepancies likely arise due to the HR-ToF-
708 AMS being unable to unambiguously resolve nitrogen-containing species, so contributions
709 from CHON and CHONS compounds are either missed or misattributed as CHO fragments.

710   This limitation biases the elemental ratios, particularly lowering O/C and therefore depressing

711   the calculated $\overline{OSc}$. Unlike the HR-ToF-AMS, the calculation of average $\overline{OSc}$ in FIGAERO-

712   CIMS and UHPLC-HRMS measurement still based on well-identified CHON compounds.

713   This structural limitation suggested that HR-ToF-AMS estimated $\overline{OSc}$ are not directly

714   comparable to FIGAERO-CIMS/UHPLC-HRMS even when all are shown in "not accounting

715   for $\overline{OS_N}$" form. The issue is especially relevant for excessive aromatic and nitrate SOA, where

716   organonitrate species (CHON, CHONS) are abundant in chamber experiments with NO_x and

717   ammonium sulphate (Surratt et al., 2007; Surratt et al., 2008; Bruns et al., 2010; Fry et al.,

718   2009). In such cases, the true $\overline{OSc}$ should be calculated as $2O/C – H/C – xN/C – yS/C$ (Kroll

719   et al., 2011). While the contribution of sulfur-containing groups is typically small, the nitrogen

720   effect is substantial in average $\overline{OSc}$ calculation.

721   Moreover, neutral losses can occur in the HR-ToF-AMS during thermal desorption, as some

722   thermally labile or highly volatile compounds can desorb as neutral fragments (e.g., CO_2 or

723   H_2O). This can also lead to an underestimation of certain oxygenated or heteroatom-containing

724   species, biasing the measured elemental ratios (e.g., O:C and N:C) and adding uncertainty to

725   the calculated average $\overline{OSc}$.

726

727   ## 4.4.   Effect of $\overline{OS_N}$ accounting on average $\overline{OSc}$ estimation in single

728   precursor system

729   This section evaluate the influence of the nitrogen correction term $(\overline{OS_N})$ on the estimated

730    $\overline{OSc}$ in single α-pinene and *o*-Cresol experiments using FIGAERO-CIMS and UHPLC-HRMS

731   measurements.

732   As noted earlier, accounting for $\overline{OS_N}$ can have non-negligible effect on the estimation of

733   average $\overline{OSc}$ of bulk SOA. Table 2 that shown below summarised the average $\overline{OSc}$ of single

734   α-pinene and o-Cresol experiments across all reactivities estimated from FIGAERO-CIMS and

735   UHPLC-HRMS measurement. This reported that ignoring $\overline{OS_N}$ term generally biases the

736   estimation of average $\overline{OSc}$ upward, leading to consistently higher average $\overline{OSc}$ values across

737   both instrument (All $\Delta\overline{OSc} < 0$).

738   In the single α-pinene experiments, the downward adjustment associated with including the

739   nitrogen correction term $(\overline{OS_N} * N/C)$ is fairly consistent across FIGAERO-CIMS and

740 UHPLC-HRMS measurement ($\Delta\overline{OSc} \approx -0.05$ to -0.2), which might suggest relatively small

741 contribution of N-containing products at the endpoints.   By contrast, the corrections are much

742 larger in the single *o*-Cresol experiments, particularly in the UHPLC-HRMS negative

743 ionisation mode ($\Delta\overline{OSc} \approx -0.43$ to -0.70) and FIGAERO-CIMS measurement ($\Delta\overline{OSc} \approx \sim 0.5$),

744 with moderate values in UHPLC-HRMS positive ionisation mode ($\Delta\overline{OSc} \approx -0.23$ to -0.29).

745 The larger adjustment in o-Cresol experiments likely arises from the fact that its oxidation is

746 dominated by nitroaromatic oxygenated compounds. These nitrogen containing species are

747 particularly well captured in the negative ion mode of UHPLC-HRMS (and also by CIMS),

748 and because of their abundance, they contribute strong influence on the $\overline{OS_N}$ ·N/C correction

749 term. As a result, their dominance drives a pronounced reduction in the estimated average $\overline{OSc}$.

750 It is important to note that, for FIGAERO-CIMS and UHPLC-HRMS, including or excluding

751 the $\overline{OS_N}$ correction term in the average $\overline{OSc}$ calculation is a deliberate choice, and its impact

752 depends strongly on the identified chemical composition of the SOA. By contrast, the HR-

753 ToF-AMS cannot resolve nitrogen-containing products, which leads to systematic

754 misattribution of CHON species as CHO fragments. This structural limitation, as discussed in

755 Section 4.3, highlights the need for caution when interpreting AMS-derived $\overline{OSc}$ values, as the

756 inability to account for $\overline{OS_N}$ can bias comparisons with FIGAERO-CIMS and UHPLC-HRMS

757 measurements.

758

759

760

761

762

763

764

765

Table 2: Average $\overline{OSc}$ for single α-pinene and o-Cresol experiments across all reactivities, estimated from FIGAERO-CIMS (hereafter CIMS), and UHPLC-HRMS (hereafter, LCMS) measurement. For FIGAERO-CIMS, values correspond to the endpoint of each experiment, while UHPLC-HRMS values are based on filter extracts collected at the experiment endpoint. $\overline{OSc}$ was estimated both accounting or not accounting the term of $\overline{OS_N}$, and the difference $\Delta\overline{OSc} = \overline{OSc}$ (accounting $\overline{OS_N}$ − $\overline{OSc}$(not accounting $\overline{OS_N}$).

Precursor	Initial Conditions (Reactivity)	Instrument	$\overline{OSc}$ (Accounting $\overline{OS_N}$)	$\overline{OSc}$ (Not accounting $\overline{OS_N}$)	$\Delta\overline{OSc}$
a-pinene	Full	CIMS	-0.57	-0.40	-0.17
		LCMS (-ve mode)	-0.58	-0.44	-0.14
		LCMS (+ve mode)	-0.99	-0.91	-0.08
	Half	CIMS	-0.52	-0.31	-0.21
		LCMS (-ve mode)	-0.61	-0.5	-0.11
		LCMS (+ve mode)	-0.92	-0.87	-0.05
	Third	CIMS	-0.46	-0.22	-0.24
		LCMS (-ve mode)	-0.45	-0.34	-0.11
		LCMS (+ve mode)	-1.21	-1.09	-0.12
o-Cresol	Full	CIMS	-0.37	0.21	-0.58
		LCMS (-ve mode)	-0.55	0.15	-0.7
		LCMS (+ve mode)	-0.66	-0.37	-0.29
	Half	CIMS	-0.21	0.27	-0.48
		LCMS (-ve mode)	-0.56	-0.13	-0.43
		LCMS (+ve mode)	-0.48	-0.25	-0.23

771

772

773

774

5. Conclusion

This study reframes the interpretation of SOA chemistry by using average $\overline{OSc}$ as a diagnostic tool to explore the evolution of SOA from both single and mixed precursor systems. Rather than focusing on detailed product identification, which has been addressed in our previous work, we emphasise how $\overline{OSc}$ trends provide broader insights into volatility, aging pathways, and precursor interactions.

We reported that average $\overline{OSc}$ generally declines as SOA mass increases in all mixed precursor systems, consistent with an increasing role of semi-volatile and less oxidised species at higher loadings from FIGAERO-CIMS measurement (accounting for $\overline{OS_N}$ correction). This behaviour seems highlights the role of $\overline{OSc}$ as a proxy for functionalisation versus fragmentation pathways and SOA volatility.

Another finding of this study is that inclusion of the $\overline{OS_N}$ correction substantially reduces average $\overline{OSc}$ estimates, particularly in *o*-Cresol experiment, which is dominate with CHON products, suggested that chemical composition and calculation choices directly influence the mechanism interpretation about SOA oxidation.

Comparisons of average $\overline{OSc}$ across FIGAERO-CIMS, UHPLC-HRMS, and HR-ToF-AMS further reveal systematic discrepancies in this study. Both the FIGAERO-CIMS and UHPLC-HRMS could identify the molecule composition, including the CHON species, whereas the HR-ToF-AMS cannot resolve nitrogen-containing species. This limitation likely results in CHON signals being misattributed as CHO, leading to introduce systematically bias to O/C and thereby the calculating $\overline{OSc}$.

Beyond instrument specific biases, the mixture precursors experiments highlight that the precursor interactions, such as OH scavenging by isoprene, NOx driven RO_2 competition, and cross interaction between RO_2 from different precursor could change the balance of functionalisation and fragmentation, producing average $\overline{OSc}$ trajectories distinct from those of single VOCs.

Data availability

All the data used in this work can be accessed on the open database of the EUROCHAMP programme (https://data.eurochamp.org/data-access/chamber-experiments/).

Competing interests

The authors declare that they have no conflict of interest.

Author contributions

GM, MRA, AV, YW and YS conceived the study. AV, YW, YS and MD conducted the experiments. TJB provided technical assistance during the experiments and contributed to the FIGAERO-CIMS data analysis. YS conducted the data analysis and wrote the manuscript with contribution from all co-authors

Acknowledgements

The Manchester Aerosol Chamber acknowledges the funding support from the European Union's Horizon 2020 research and innovation programme under grant agreement no. 730997, which supports the EUROCHAMP2020 research programme. Instrumentational support was funded by the NERC Atmospheric Measurement and Observational Facility (AMOF). Y.W. acknowledges the joint scholarship of The University of Manchester and Chinese Scholarship Council. M.R.A. acknowledges funding support by UK National Centre for Atmospheric Sciences (NACS). A.V. acknowledges the funding support by Natural Environment Research Council (NERC) EAO Doctoral Training Partnership. The authors would also like to thank Kelly Pereira for on-site UHPLC-HRMS training for filter analysis and for providing the automated non-targeted analysis method for UHPLC-HRMS. I acknowledge the use of ChatGPT AI tool to proof-reading and correct grammar at the final stage of the writing process for this paper, which I reviewed, edited, and take full responsibility for. All final wording reflects my own edits and judgment.

830 Reference:

831 Ahlberg, E., Falk, J., Eriksson, A., Holst, T., Brune, W. H., Kristensson, A., Roldin, P., and
832 Svenningsson, B.: Secondary organic aerosol from VOC mixtures in an oxidation flow
833 reactor, Atmospheric Environment, 161, 210-220,
834 https://doi.org/10.1016/j.atmosenv.2017.05.005, 2017.
835 Aiken, A. C., DeCarlo, P. F., Kroll, J. H., Worsnop, D. R., Huffman, J. A., Docherty, K. S.,
836 Ulbrich, I. M., Mohr, C., Kimmel, J. R., Sueper, D., Sun, Y., Zhang, Q., Trimborn, A.,
837 Northway, M., Ziemann, P. J., Canagaratna, M. R., Onasch, T. B., Alfarra, M. R., Prevot,
838 A. S. H., Dommen, J., Duplissy, J., Metzger, A., Baltensperger, U., and Jimenez, J. L.: O/C
839 and OM/OC Ratios of Primary, Secondary, and Ambient Organic Aerosols with High-
840 Resolution Time-of-Flight Aerosol Mass Spectrometry, Environmental Science &
841 Technology, 42, 4478-4485, 10.1021/es703009q, 2008.
842 Alfarra, M. R., Coe, H., Allan, J. D., Bower, K. N., Boudries, H., Canagaratna, M. R.,
843 Jimenez, J. L., Jayne, J. T., Garforth, A. A., Li, S.-M., and Worsnop, D. R.: Characterization
844 of urban and rural organic particulate in the Lower Fraser Valley using two Aerodyne
845 Aerosol Mass Spectrometers, Atmospheric Environment, 38, 5745-5758,
846 https://doi.org/10.1016/j.atmosenv.2004.01.054, 2004.
847 Atkinson, R. B., D. L. Cox, R. A.Crowley, J. N.Hampson, R. F.Hynes, R. G.Jenkin, M.
848 E.Rossi, M. J.Troe, J.: Evaluated kinetic and photochemical data for atmospheric
849 chemistry: Volume I - gas phase reactions of Ox, HOx, NOxand SOxspecies, Atmos.
850 Chem. Phys., 4, 1738, 10.5194/acp-4-1461-2004, 2004.
851 Bruns, E. A., Perraud, V., Zelenyuk, A., Ezell, M. J., Johnson, S. N., Yu, Y., Imre, D.,
852 Finlayson-Pitts, B. J., and Alexander, M. L.: Comparison of FTIR and Particle Mass
853 Spectrometry for the Measurement of Particulate Organic Nitrates, Environmental
854 Science & Technology, 44, 1056-1061, 10.1021/es9029864, 2010.
855 Carlton, A. G., Wiedinmyer, C., and Kroll, J. H.: A review of Secondary Organic Aerosol
856 (SOA) formation from isoprene, Atmos. Chem. Phys., 9, 4987-5005, 10.5194/acp-9-
857 4987-2009, 2009.
858 Chen, X., Li, K., Li, R., Fang, L., Bian, H., Jiang, W., Yan, C., and Du, L.: NOx-driven
859 chemical transformation of terpene mixtures: Linking highly oxygenated organic
860 molecules to health effects in secondary organic aerosol, Journal of Environmental
861 Sciences, https://doi.org/10.1016/j.jes.2025.09.004, 2025.
862 Chhabra, P. S., Flagan, R. C., and Seinfeld, J. H.: Elemental analysis of chamber organic
863 aerosol using an aerodyne high-resolution aerosol mass spectrometer, Atmos. Chem.
864 Phys., 10, 4111-4131, 10.5194/acp-10-4111-2010, 2010.
865 Cui, Y., Chen, K., Zhang, H., Lin, Y.-H., and Bahreini, R.: Chemical Composition and
866 Optical Properties of Secondary Organic Aerosol from Photooxidation of Volatile
867 Organic Compound Mixtures, ACS ES&T Air, 1, 247-258, 10.1021/acsestair.3c00041,
868 2024.
869 D. Sueper and collaborators, 2020. ToF-AMS Data Analysis Software Webpage,
870 http://cires1.colorado.edu/jimenez-group/wiki/index.php/ToF-AMS_Analysis_Software
871 D'Ambro, E. L., Schobesberger, S., Gaston, C. J., Lopez-Hilfiker, F. D., Lee, B. H., Liu, J.,
872 Zelenyuk, A., Bell, D., Cappa, C. D., Helgestad, T., Li, Z., Guenther, A., Wang, J., Wise,
873 M., Caylor, R., Surratt, J. D., Riedel, T., Hyttinen, N., Salo, V. T., Hasan, G., Kurtén, T.,
874 Shilling, J. E., and Thornton, J. A.: Chamber-based insights into the factors controlling

epoxydiol (IEPOX) secondary organic aerosol (SOA) yield, composition, and volatility, Atmos. Chem. Phys., 19, 11253-11265, 10.5194/acp-19-11253-2019, 2019.

D'Ambro, E. L., Schobesberger, S., Gaston, C. J., Lopez-Hilfiker, F. D., Lee, B. H., Liu, J., Zelenyuk, A., Bell, D., Cappa, C. D., Helgestad, T., Li, Z., Guenther, A., Wang, J., Wise, M., Caylor, R., Surratt, J. D., Riedel, T., Hyttinen, N., Salo, V. T., Hasan, G., Kurtén, T., Shilling, J. E., and Thornton, J. A.: Chamber-based insights into the factors controlling epoxydiol (IEPOX) secondary organic aerosol (SOA) yield, composition, and volatility, Atmos. Chem. Phys., 19, 11253-11265, 10.5194/acp-19-11253-2019, 2019.

Daumit, K. E., Kessler, S. H., and Kroll, J. H.: Average chemical properties and potential formation pathways of highly oxidized organic aerosol, Faraday Discuss, 165, 181-202, 10.1039/c3fd00045a, 2013.

DeCarlo, P. F., Kimmel, J. R., Trimborn, A., Northway, M. J., Jayne, J. T., Aiken, A. C., Gonin, M., Fuhrer, K., Horvath, T., Docherty, K. S., Worsnop, D. R., and Jimenez, J. L.: Field-Deployable, High-Resolution, Time-of-Flight Aerosol Mass Spectrometer, Analytical Chemistry, 78, 8281-8289, 10.1021/ac061249n, 2006.

Dillon, T. J., Dulitz, K., Groß, C. B. M., and Crowley, J. N.: Temperature-dependent rate coefficients for the reactions of the hydroxyl radical with the atmospheric biogenics isoprene, alpha-pinene and delta-3-carene, Atmos. Chem. Phys., 17, 15137-15150, 10.5194/acp-17-15137-2017, 2017.

Docherty, K. S., Corse, E. W., Jaoui, M., Offenberg, J. H., Kleindienst, T. E., Krug, J. D., Riedel, T. P., and Lewandowski, M.: Trends in the oxidation and relative volatility of chamber-generated secondary organic aerosol, Aerosol Science and Technology, 52, 992-1004, 10.1080/02786826.2018.1500014, 2018.

Du, M., Voliotis, A., Shao, Y., Wang, Y., Bannan, T. J., Pereira, K. L., Hamilton, J. F., Percival, C. J., Alfarra, M. R., and McFiggans, G.: Combined application of Online FIGAERO-CIMS and Offline LC-Orbitrap MS to Characterize the Chemical Composition of SOA in Smog Chamber Studies, Atmos. Meas. Tech. Discuss., 2021, 1-42, 10.5194/amt-2021-420, 2021.

Eddingsaas, N. C., Loza, C. L., Yee, L. D., Chan, M., Schilling, K. A., Chhabra, P. S., Seinfeld, J. H., and Wennberg, P. O.: α-pinene photooxidation under controlled chemical conditions – Part 2: SOA yield and composition in low- and high-NO_x environments, Atmos. Chem. Phys., 12, 7413-7427, 10.5194/acp-12-7413-2012, 2012.

Fry, J. L., Kiendler-Scharr, A., Rollins, A. W., Wooldridge, P. J., Brown, S. S., Fuchs, H., Dubé, W., Mensah, A., dal Maso, M., Tillmann, R., Dorn, H. P., Brauers, T., and Cohen, R. C.: Organic nitrate and secondary organic aerosol yield from NO_3 oxidation of β-pinene evaluated using a gas-phase kinetics/aerosol partitioning model, Atmos. Chem. Phys., 9, 1431-1449, 10.5194/acp-9-1431-2009, 2009.

Han, S., Li, Z., Lau, Y. S., Xiao, Y., Miljevic, B., Horchler, J., Li, J., Hu, W.-P., Wang, H., Wang, B., and Ristovski, Z.: Unraveling secondary organic aerosol formation from isoprene and toluene mixture, npj Climate and Atmospheric Science, 8, 311, 10.1038/s41612-025-01189-4, 2025.

Hildebrandt, L., Henry, K. M., Kroll, J. H., Worsnop, D. R., Pandis, S. N., and Donahue, N. M.: Evaluating the Mixing of Organic Aerosol Components Using High-Resolution Aerosol Mass Spectrometry, Environmental Science & Technology, 45, 6329-6335, 10.1021/es200825g, 2011.

921 Hoffmann, T., Huang, R.-J., and Kalberer, M.: Atmospheric Analytical Chemistry,
922 Analytical Chemistry, 83, 4649-4664, 10.1021/ac2010718, 2011.
923 Hoffmann, T., Odum, J. R., Bowman, F., Collins, D., Klockow, D., Flagan, R. C., and
924 Seinfeld, J. H.: Formation of Organic Aerosols from the Oxidation of Biogenic
925 Hydrocarbons, Journal of Atmospheric Chemistry, 26, 189-222,
926 10.1023/A:1005734301837, 1997.
927 Jayne, J. T., Leard, D. C., Zhang, X., Davidovits, P., Smith, K. A., Kolb, C. E., and
928 Worsnop, D. R.: Development of an aerosol mass spectrometer for size and
929 composition analysis of submicron particles, Aerosol Science & Technology, 33, 49-70,
930 2000.
931 Jimenez, J. L., Jayne, J. T., Shi, Q., Kolb, C. E., Worsnop, D. R., Yourshaw, I., Seinfeld, J.
932 H., Flagan, R. C., Zhang, X., Smith, K. A., Morris, J. W., and Davidovits, P.: Ambient
933 aerosol sampling using the Aerodyne Aerosol Mass Spectrometer, Journal of
934 Geophysical Research: Atmospheres, 108, https://doi.org/10.1029/2001JD001213,
935 2003.
936 Kroll, J. H., Lim, C. Y., Kessler, S. H., and Wilson, K. R.: Heterogeneous Oxidation of
937 Atmospheric Organic Aerosol: Kinetics of Changes to the Amount and Oxidation State
938 of Particle-Phase Organic Carbon, The Journal of Physical Chemistry A, 119, 10767-
939 10783, 10.1021/acs.jpca.5b06946, 2015.
940 Kroll, J. H., Ng, N. L., Murphy, S. M., Flagan, R. C., and Seinfeld, J. H.: Secondary organic
941 aerosol formation from isoprene photooxidation under high-NOx conditions,
942 Geophysical Research Letters, 32, https://doi.org/10.1029/2005GL023637, 2005a.
943 Kroll, J. H., Ng, N. L., Murphy, S. M., Varutbangkul, V., Flagan, R. C., and Seinfeld, J. H.:
944 Chamber studies of secondary organic aerosol growth by reactive uptake of simple
945 carbonyl compounds, Journal of Geophysical Research: Atmospheres, 110,
946 https://doi.org/10.1029/2005JD006004, 2005b.
947 Kroll, J. H., Donahue, N. M., Jimenez, J. L., Kessler, S. H., Canagaratna, M. R., Wilson, K.
948 R., Altieri, K. E., Mazzoleni, L. R., Wozniak, A. S., Bluhm, H., Mysak, E. R., Smith, J. D.,
949 Kolb, C. E., and Worsnop, D. R.: Carbon oxidation state as a metric for describing the
950 chemistry of atmospheric organic aerosol, Nature Chemistry, 3, 133-139,
951 10.1038/nchem.948, 2011.
952 Lee, B.-H., Pierce, J. R., Engelhart, G. J., and Pandis, S. N.: Volatility of secondary
953 organic aerosol from the ozonolysis of monoterpenes, Atmospheric Environment, 45,
954 2443-2452, https://doi.org/10.1016/j.atmosenv.2011.02.004, 2011.
955 Lee, B. H., Lopez-Hilfiker, F. D., Mohr, C., Kurtén, T., Worsnop, D. R., and Thornton, J. A.:
956 An Iodide-Adduct High-Resolution Time-of-Flight Chemical-Ionization Mass
957 Spectrometer: Application to Atmospheric Inorganic and Organic Compounds,
958 Environmental Science & Technology, 48, 6309-6317, 10.1021/es500362a, 2014.
959 Li, K., Zhang, X., Zhao, B., Bloss, W. J., Lin, C., White, S., Yu, H., Chen, L., Geng, C.,
960 Yang, W., Azzi, M., George, C., and Bai, Z.: Suppression of anthropogenic secondary
961 organic aerosol formation by isoprene, npj Climate and Atmospheric Science, 5, 12,
962 10.1038/s41612-022-00233-x, 2022.
963 Lopez-Hilfiker, F. D., Mohr, C., Ehn, M., Rubach, F., Kleist, E., Wildt, J., Mentel, T. F.,
964 Lutz, A., Hallquist, M., Worsnop, D., and Thornton, J. A.: A novel method for online
965 analysis of gas and particle composition: description and evaluation of a Filter Inlet for
966 Gases and AEROsols (FIGAERO), Atmos. Meas. Tech., 7, 983-1001, 10.5194/amt-7-983-
967 2014, 2014.

McFiggans, G., Mentel, T. F., Wildt, J., Pullinen, I., Kang, S., Kleist, E., Schmitt, S., Springer, M., Tillmann, R., and Wu, C.: Secondary organic aerosol reduced by mixture of atmospheric vapours, Nature, 565, 587, 2019.

Pandis, S. N., Paulson, S. E., Seinfeld, J. H., and Flagan, R. C.: Aerosol formation in the photooxidation of isoprene and β-pinene, Atmospheric Environment. Part A. General Topics, 25, 997-1008, https://doi.org/10.1016/0960-1686(91)90141-S, 1991.

Pereira, K., Ward, M., Wilkinson, J., Sallach, J., Bryant, D., Dixon, W., Hamilton, J., and Lewis, A.: An Automated Methodology for Non-targeted Compositional Analysis of Small Molecules in High Complexity Environmental Matrices Using Coupled Ultra Performance Liquid Chromatography Orbitrap Mass Spectrometry, Environmental Science & Technology, XXXX, 10.1021/acs.est.0c08208, 2021.

Presto, A. A., Miracolo, M. A., Kroll, J. H., Worsnop, D. R., Robinson, A. L., and Donahue, N. M.: Intermediate-Volatility Organic Compounds: A Potential Source of Ambient Oxidized Organic Aerosol, Environmental Science & Technology, 43, 4744-4749, 10.1021/es803219q, 2009.

Pullinen, I., Schmitt, S., Kang, S., Sarrafzadeh, M., Schlag, P., Andres, S., Kleist, E., Mentel, T. F., Rohrer, F., Springer, M., Tillmann, R., Wildt, J., Wu, C., Zhao, D., Wahner, A., and Kiendler-Scharr, A.: Impact of NOx on secondary organic aerosol (SOA) formation from α-pinene and β-pinene photooxidation: the role of highly oxygenated organic nitrates, Atmos. Chem. Phys., 20, 10125-10147, 10.5194/acp-20-10125-2020, 2020.

Shao, Y., Voliotis, A., Du, M., Wang, Y., Pereira, K., Hamilton, J., Alfarra, M. R., and McFiggans, G.: Chemical composition of secondary organic aerosol particles formed from mixtures of anthropogenic and biogenic precursors, Atmos. Chem. Phys., 22, 9799-9826, 10.5194/acp-22-9799-2022, 2022a.

Shao, Y., Wang, Y., Du, M., Voliotis, A., Alfarra, M. R., O'Meara, S. P., Turner, S. F., and McFiggans, G.: Characterisation of the Manchester Aerosol Chamber facility, Atmos. Meas. Tech., 15, 539-559, 10.5194/amt-15-539-2022, 2022b.

Shilling, J. E., Chen, Q., King, S. M., Rosenoern, T., Kroll, J. H., Worsnop, D. R., DeCarlo, P. F., Aiken, A. C., Sueper, D., Jimenez, J. L., and Martin, S. T.: Loading-dependent elemental composition of α-pinene SOA particles, Atmos. Chem. Phys., 9, 771-782, 10.5194/acp-9-771-2009, 2009.

Stark, H., Yatavelli, R. L. N., Thompson, S. L., Kimmel, J. R., Cubison, M. J., Chhabra, P. S., Canagaratna, M. R., Jayne, J. T., Worsnop, D. R., and Jimenez, J. L.: Methods to extract molecular and bulk chemical information from series of complex mass spectra with limited mass resolution, International Journal of Mass Spectrometry, 389, 26-38, https://doi.org/10.1016/j.ijms.2015.08.011, 2015.

Stroud, C. A., Roberts, J. M., Goldan, P. D., Kuster, W. C., Murphy, P. C., Williams, E. J., Hereid, D., Parrish, D., Sueper, D., Trainer, M., Fehsenfeld, F. C., Apel, E. C., Riemer, D., Wert, B., Henry, B., Fried, A., Martinez-Harder, M., Harder, H., Brune, W. H., Li, G., Xie, H., and Young, V. L.: Isoprene and its oxidation products, methacrolein and methylvinyl ketone, at an urban forested site during the 1999 Southern Oxidants Study, Journal of Geophysical Research: Atmospheres, 106, 8035-8046, https://doi.org/10.1029/2000JD900628, 2001.

Surratt, J. D., Kroll, J. H., Kleindienst, T. E., Edney, E. O., Claeys, M., Sorooshian, A., Ng, N. L., Offenberg, J. H., Lewandowski, M., Jaoui, M., Flagan, R. C., and Seinfeld, J. H.:

1014   Evidence for Organosulfates in Secondary Organic Aerosol, Environmental Science &
1015   Technology, 41, 517-527, 10.1021/es062081q, 2007.
1016   Surratt, J. D., Gómez-González, Y., Chan, A. W. H., Vermeylen, R., Shahgholi, M.,
1017   Kleindienst, T. E., Edney, E. O., Offenberg, J. H., Lewandowski, M., Jaoui, M., Maenhaut,
1018   W., Claeys, M., Flagan, R. C., and Seinfeld, J. H.: Organosulfate Formation in Biogenic
1019   Secondary Organic Aerosol, The Journal of Physical Chemistry A, 112, 8345-8378,
1020   10.1021/jp802310p, 2008.
1021   Voliotis, A., Wang, Y., Shao, Y., Du, M., Bannan, T. J., Percival, C. J., Pandis, S. N.,
1022   Alfarra, M. R., and McFiggans, G.: Exploring the composition and volatility of secondary
1023   organic aerosols in mixed anthropogenic and biogenic precursor systems, Atmos.
1024   Chem. Phys. Discuss., 2021, 1-39, 10.5194/acp-2021-215, 2021.
1025   Voliotis, A., Du, M., Wang, Y., Shao, Y., Bannan, T. J., Flynn, M., Pandis, S. N., Percival,
1026   C. J., Alfarra, M. R., and McFiggans, G.: The influence of the addition of isoprene on the
1027   volatility of particles formed from the photo-oxidation of anthropogenic–biogenic
1028   mixtures, Atmos. Chem. Phys., 22, 13677-13693, 10.5194/acp-22-13677-2022, 2022a.
1029   Voliotis, A., Du, M., Wang, Y., Shao, Y., Alfarra, M. R., Bannan, T. J., Hu, D., Pereira, K. L.,
1030   Hamilton, J. F., Hallquist, M., Mentel, T. F., and McFiggans, G.: Chamber investigation of
1031   the formation and transformation of secondary organic aerosol in mixtures of biogenic
1032   and anthropogenic volatile organic compounds, Atmos. Chem. Phys. Discuss., 2022, 1-
1033   49, 10.5194/acp-2021-1080, 2022b.
1034   Wennberg, P. O., Bates, K. H., Crounse, J. D., Dodson, L. G., McVay, R. C., Mertens, L.
1035   A., Nguyen, T. B., Praske, E., Schwantes, R. H., Smarte, M. D., St Clair, J. M., Teng, A. P.,
1036   Zhang, X., and Seinfeld, J. H.: Gas-Phase Reactions of Isoprene and Its Major Oxidation
1037   Products, Chemical Reviews, 118, 3337-3390, 10.1021/acs.chemrev.7b00439, 2018.
1038   Winterhalter, R., Van Dingenen, R., Larsen, B. R., Jensen, N. R., and Hjorth, J.: LC-MS
1039   analysis of aerosol particles from the oxidation of α-pinene by ozone and OH-
1040   radicals, Atmos. Chem. Phys. Discuss., 2003, 1-39, 10.5194/acpd-3-1-2003, 2003.
1041   Xu, L., Middlebrook, A. M., Liao, J., de Gouw, J. A., Guo, H., Weber, R. J., Nenes, A.,
1042   Lopez-Hilfiker, F. D., Lee, B. H., Thornton, J. A., Brock, C. A., Neuman, J. A., Nowak, J. B.,
1043   Pollack, I. B., Welti, A., Graus, M., Warneke, C., and Ng, N. L.: Enhanced formation of
1044   isoprene-derived organic aerosol in sulfur-rich power plant plumes during Southeast
1045   Nexus, Journal of Geophysical Research: Atmospheres, 121, 11,137-111,153,
1046   10.1002/2016jd025156, 2016.
1047   Zhao, Y., Zhao, Y., Wang, C., Shao, Y., Xie, H., Yang, J., Zhang, W., Wu, G., Li, G., Jiang,
1048   L., and Yang, X.: Photooxidation and ozonolysis of α-pinene and limonene mixtures:
1049   Mechanisms of secondary organic aerosol formation and cross-dimerization, Journal of
1050   Environmental Sciences, https://doi.org/10.1016/j.jes.2025.04.020, 2025.
1051